PERSPECTIVE | DECEMBER 23 2024

Perspectives on epitaxial InGaP for quantum and nonlinear optics

Joshua Akin ; Yunlei Zhao; A. K. M. Naziul Haque ; Kejie Fang

Appl. Phys. Lett. 125, 260501 (2024)
https://doi.org/10.1063/5.0241224

Applied Physics Letters PERSPECTIVE pubs.aip.org/aip/apl

Perspectives on epitaxial InGaP for quantum and nonlinear optics

Cite as: Appl. Phys. Lett. **125**, 260501 (2024); doi: 10.1063/5.0241224
Submitted: 29 September 2024 · Accepted: 4 December 2024 ·
Published Online: 23 December 2024

Joshua Akin,[1,2] Yunlei Zhao,[1,2] A. K. M. Naziul Haque,[1,2] and Kejie Fang[1,2,a)]

AFFILIATIONS

[1]Holonyak Micro and Nanotechnology Laboratory and Department of Electrical and Computer Engineering, University of Illinois at Urbana-Champaign, Urbana, Illinois 61801 USA
[2]Illinois Quantum Information Science and Technology Center, University of Illinois at Urbana-Champaign, Urbana, Illinois 61801 USA

[a)]Author to whom correspondence should be addressed: kfang3@illinois.edu

ABSTRACT

Nonlinear optical materials are essential for the development of both nonlinear and quantum optics and have advanced recently from bulk crystals to integrated material platforms. In this Perspective, we provide an overview of the emerging InGaP $\chi^{(2)}$ nonlinear integrated photonics platform and its experimental achievements. With its exceptional $\chi^{(2)}$ nonlinearity and low optical losses, the epitaxial InGaP platform significantly enhances a wide range of second-order nonlinear optical effects, from second-harmonic generation to entangled photon pair sources, achieving efficiencies several orders of magnitude beyond the current state of the art. Moreover, the InGaP platform enables quantum nonlinear optics at the few- and single-photon levels via passive nonlinearities, which has broad implications for quantum information processing and quantum networking. We also examine the current limitations of the InGaP platform and propose potential solutions to fully unlock its capabilities.

I. INTRODUCTION

Nonlinear optical materials play a pivotal role in advancing both nonlinear optics and quantum optics. In addition to their classical uses, such as in optical parametric oscillators[1] and high-harmonic generation,[2,3] nonlinear crystals have long been employed to generate quantum light, including entangled photon pairs[4] and squeezed light.[5] These quantum light sources are foundational to the experimental progress in quantum communications,[6] quantum sensing,[7] and quantum computing.[8]

In recent years, nonlinear optical materials have progressed from bulk crystals to integrated material platforms, driven by advances in material growth and fabrication techniques. These developments have facilitated the use of materials with higher nonlinear susceptibilities and the creation of light-confining nanophotonic structures, resulting in a substantial increase in nonlinear optical efficiencies.[9] Figure 1 summarizes several leading second-order ($\chi^{(2)}$) nonlinear thin-film materials, including their second-order susceptibility and transparency window. Among them, III–V materials, including $Al_xGa_{1-x}As$ and $In_{0.5}Ga_{0.5}P$ (InGaP), exhibit the highest $\chi^{(2)}$ susceptibilities and a broad transparency window. They can be epitaxially grown on the GaAs substrate, leading to versatile III–V integrated photonics platforms. In the case of $Al_xGa_{1-x}As$, increasing the aluminum composition expands the bandgap, but this also results in a marked decrease in the second-order susceptibility.[10] Moreover, arsenic-based III–V materials suffer from strong optical absorption at wavelengths below 800 nm,[11,12] due to the antibonding As–As surface state that lies below the bandgap.[13] These limitations have made $Al_xGa_{1-x}As$ a less suitable choice for second-order nonlinear optics involving light in the telecommunication band and the corresponding second harmonics.

In this Perspective, we provide an overview of the emerging InGaP $\chi^{(2)}$ nonlinear integrated photonics platform and discuss its unique advantages for nonlinear and quantum optics involving the telecommunication band. In Sec. II, we discuss the material properties of InGaP. Section III discusses properties of InGaP nonlinear photonic devices, including microring resonators and waveguides. Sections IV and V discuss nonlinear and quantum optical effects of the cavity and waveguide, respectively. Finally, we briefly examine the current limitations of the InGaP platform and propose potential solutions.

II. INGAP AS A PRIME NONLINEAR MATERIAL

InGaP is a III–V semiconductor material that is lattice-matched to GaAs. As a result, thin-film single-crystalline InGaP can be

epitaxially grown on the GaAs substrate via metal-organic chemical vapor deposition (MOCVD) or molecular beam epitaxy (MBE). Due to its high electron mobility, direct bandgap, and thermal stability, InGaP has been used for applications including solar cells,[16] LEDs,[17] photon detectors,[18] heterojunction bipolar transistors,[19] and high-electron-mobility transistors.[20] In addition, thin-film InGaP has also been studied for nonlinear optics by exploiting its large Kerr nonlinearity,[21,22] leading to the demonstration of frequency combs,[23] optical parametric oscillators,[24] and entangled photon generation via four-wave mixing.[25]

Remarkably, InGaP also possesses a large second-order susceptibility ($\chi^{(2)}_{xyz} = 220$ pm/V)[26] and a bandgap of 1.92 eV corresponding to a cutoff wavelength of 645 nm. This marks InGaP as another thin-film material, besides $Al_xGa_{1-x}As$ ($x \approx 0.3$), that has the highest second-order susceptibility as well as a cutoff wavelength less than the second harmonics of the telecommunication C band light. However, what makes InGaP unique for second-order nonlinear optics involving the telecommunication C band light is the fact that its antibonding anion state lies well above the bandgap,[13] which avoids anion state-induced absorption below the bandgap. In contrast, the antibonding As–As surface state of $Al_xGa_{1-x}As$ lies below its bandgap,[13] resulting in strong optical absorption at wavelengths shorter than 800 nm.[11,12] In addition, the transparency window of InGaP extends to ~11 μm,[27] which will enable applications in the mid-infrared wavelength band, including optical parametric oscillators,[28,29] detectors,[30] and quantum cascade lasers.[31]

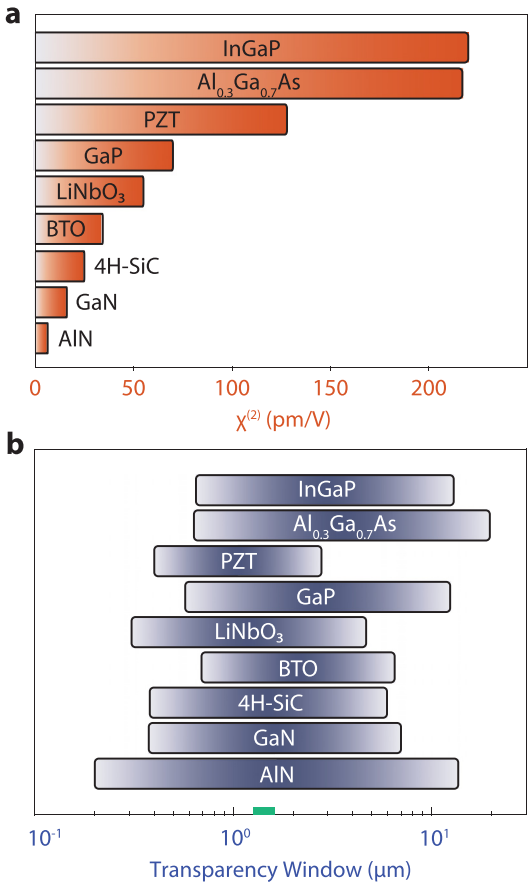

FIG. 1. $\chi^{(2)}$ susceptibility (a) and transparency window (b) of leading thin-film second-order nonlinear materials. The green bar on the x axis of (b) denotes the optical telecommunication band from 1260 to 1625 nm.

III. INGAP NONLINEAR PHOTONIC INTEGRATED CIRCUITS

Because InGaP has a similar refractive index as the GaAs substrate from which it is grown, in order to confine light in the InGaP thin-film photonic structures, it needs to be separated from the GaAs substrate. This can be achieved by transferring the InGaP thin film to a low-index substrate using various wafer bonding methods, including adhesive bonding[14] and, more recently, low-temperature plasma-activated bonding,[15] as shown in Fig. 2(a). However, wafer bonding or flip-chip bonding can be challenging, requiring special tools and complicated processing. Instead, we developed a transfer-free method that makes suspended InGaP photonic integrated circuits in the InGaP-on-GaAs platform. The fabrication process is illustrated in Fig. 2(b). Starting from the InGaP-on-GaAs epitaxial stack, the device pattern is defined using electron beam lithography and transferred to the InGaP thin film via inductively coupled plasma reactive-ion etch (ICP-RIE) using a mixture of $Cl_2/CH_4/Ar$ gas. Then, a thin layer of Al_2O_3 is deposited on the sample via atomic layer deposition (ALD), followed by patterning the releasing holes in the Al_2O_3 layer. Finally, the InGaP device is released from the GaAs substrate using selective wet etching. More details of the fabrication process are provided in Refs. 32 and 33. Figures 2(c) and 2(d) show scanning electron microscope (SEM) images of the fabricated InGaP photonic integrated circuits, including waveguide-coupled microring resonators and meander waveguides.

A. Microring resonators

In order to exploit the second-order susceptibility $\chi^{(2)}_{xyz}$ of InGaP for second-order nonlinear optics, transverse-electric modes (TE_{00}) and transverse-magnetic modes (TM_{00}) of the microring resonator are used for the fundamental and second harmonics, respectively. The fundamental-harmonic (FH) and second-harmonic (SH) modes, a and b, satisfy the frequency- and phase-matching conditions:[32] $\omega_b = 2\omega_a$ and $m_b = 2m_a \pm 2$, where m_k is the azimuthal number of mode k. This can be achieved by designing the width of the microring for a given InGaP thickness. For phase matching between the telecommunication band FH mode and the corresponding SH mode, the thickness of InGaP should be around 115 nm.[32] The phase-matching width is sensitive to the InGaP thickness: 1 nm change of InGaP thickness results in approximately 80 nm change in the phase-matching width of a 5-μm-radius ring.[32] In practice, we find the SEM-measured film thickness is reliable and use it to design the microring. In addition, an array of microrings with sweeping width is fabricated to ensure the phase matching is realized in one of the microrings in the presence of thickness uncertainty.

The quality factor of the InGaP microring resonator depends on the ALD material used to suspend the microring resonator.[33] The intrinsic quality factor (Q_{ai}) of 1550 nm band TE_{00} resonances of the fabricated microring with 5 μm radius and 1 μm width is $4 - 6 \times 10^5$ for ALD Al_2O_3, which is approximately $2 - 3\times$ higher than that of microring resonators with ALD SiO_2. This is likely due to the passivation effect of Al_2O_3.[34] The intrinsic quality factor of 775 nm band

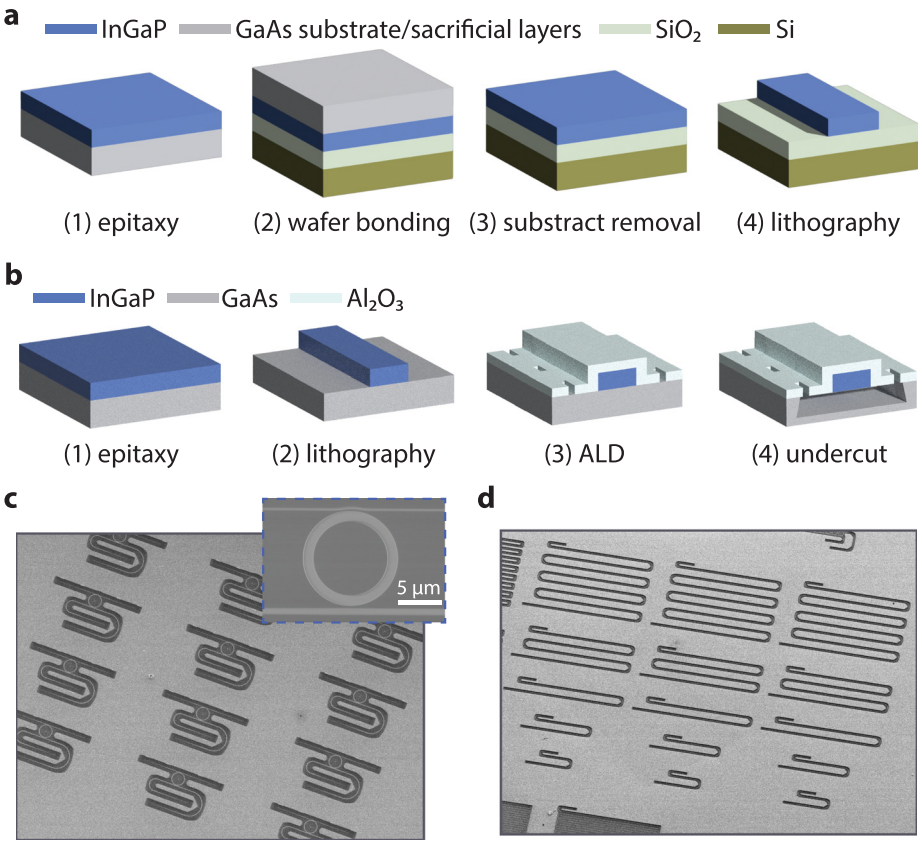

FIG. 2. (a). Illustration of the fabrication process of the InGaP-on-insulator photonic integrated circuits via wafer bonding, including adhesive bonding[14] and low-temperature plasma-activated bonding.[15] (b) Illustration of the fabrication process of the suspended InGaP photonic integrated circuit. (c) SEM images of waveguide-coupled microring resonators. (d) SEM image of waveguide devices.

TM_{00} resonances of the same microring is $1–2 \times 10^5$ and is nearly independent of the ALD material. Efficient second-harmonic generation (SHG) is realized in phase-matched InGaP microrings with an efficiency of 440 000%/W,[33] in comparison with recent demonstrations using lithium niobate microrings.[35,36]

The nonlinear interaction between the FH and SH modes can be described by the Hamiltonian, $\hat{H} = g(\hat{a}^2\hat{b}^\dagger + \hat{a}^{\dagger 2}\hat{b})$, where $\hat{a}(\hat{b})$ and $\hat{a}^\dagger(\hat{b}^\dagger)$ are the annihilation and creation operators for mode $a(b)$. The nonlinear coupling g is inferred from the SHG efficiency of the microring. For the phase-matched 5 μm-radius microring, we find $g/2\pi \approx 11$ MHz,[32] which is consistent with the simulation. The nonlinear coupling scales with the microring radius approximately as $g \propto \frac{1}{\sqrt{R}}$.

TABLE I. Cavity $\chi^{(2)}$ process. SPDC: spontaneous parametric downconversion. OPO: optical parametric oscillation. Pump power for squeezed light is assumed for optimal quadrature noise squeezing (i.e., $\kappa_{a,i}/\kappa_a$) on resonance. Critical coupling ($\kappa_i = \kappa/2$) is assumed.

$\chi^{(2)}$ process	Metric	Scaling
SHG	Efficiency	$g^2/\kappa_{ai}^2\kappa_{bi}$ (Ref. 37)
SPDC	Pair generation rate	$g^2/\kappa_{ai}\kappa_{bi}$ (Ref. 38)
OPO	Pump threshold	$\kappa_{ai}^2\kappa_{bi}/g^2$ (Ref. 39)
Squeezed light	Pump power	$\kappa_{ai}^2\kappa_{bi}/g^2$ (Ref. 39)

A nonlinearity-to-loss ratio, g/κ_{ai}, where $\kappa_{ai} \equiv \omega_a/Q_{ai}$, can be defined to characterize the nonlinear cavity. Almost all second-order nonlinear optical effects of the cavity are determined by this ratio. Table I summarizes the relation between the key metrics of several nonlinear optical processes and the nonlinearity-to-loss ratio. The 5 μm-radius InGaP microring with $Q_{ai} = 6 \times 10^5$ achieves a high $g/\kappa_{ai} = 3.5\%$. In Fig. 3(a), we compare the nonlinearity-to-loss ratio of the state-of-the-art InGaP microring with microring resonators made in other $\chi^{(2)}$ nonlinear photonics platforms.

B. Waveguides

Broadband second-order nonlinear optical effects can be realized in waveguides as opposed to microring resonators. Similar to the microring resonator, TE_{00} and TM_{00} modes of the waveguide are used for the fundamental and second harmonics, respectively. By designing the waveguide width for a given InGaP thickness, the two modes can satisfy the frequency- and phase-matching conditions: $\omega_b = 2\omega_a$ and $k_b = 2k_a$, which lead to $n_b = n_a$, where n_k is the effective mode index of mode k.

The phase-matched nonlinear waveguide can be characterized by its loss and nonlinear efficiency. The loss of the TE_{00} mode of the InGaP waveguide in the 1550 nm band is measured to be $\gamma = 0.8 \pm 0.4$ dB/cm,[33] which is consistent with the intrinsic quality factor of the microring resonator (corresponding to 0.4 dB/cm). The difference might be due to the uncertainty of the fiber-optic coupling efficiency when

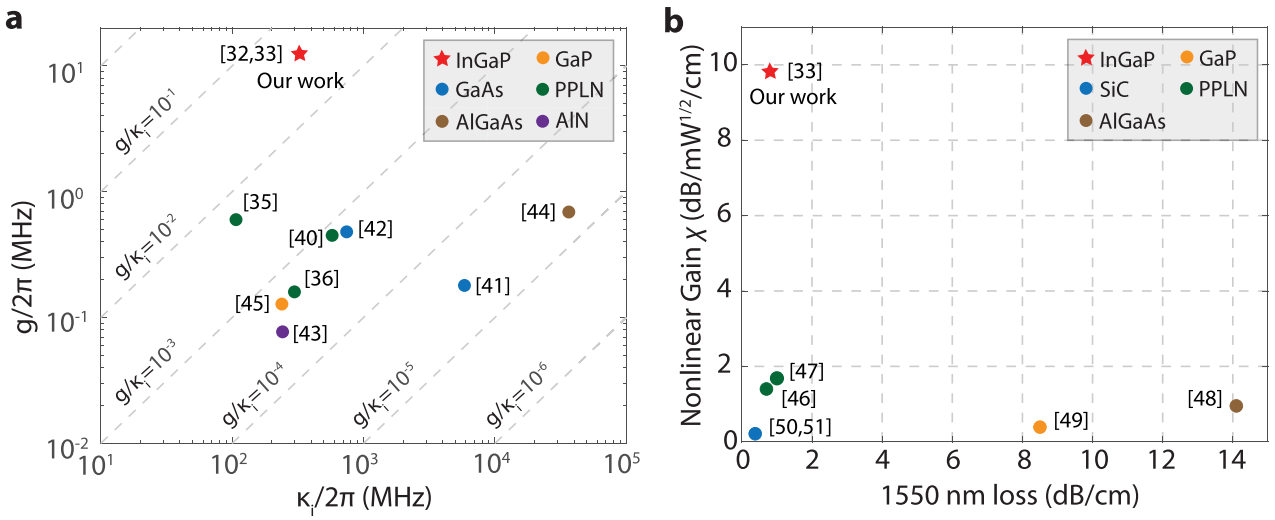

FIG. 3. (a) Nonlinear mode coupling coefficient (g) and intrinsic photon loss rate of the fundamental mode (κ_i) of microring resonators made in second-order nonlinear photonics platforms, including InGaP,[32,33] PPLN,[35,36,40] GaAs,[41,42] AlN,[43] AlGaAs,[44] GaP.[45] (b) Nonlinear gain χ and 1550 nm wavelength band loss of nanophotonic waveguides made in second-order nonlinear photonics platforms. InGaP,[33] PPLN,[46,47] AlGaAs,[48] GaP,[49] and SiC.[50,51]

TABLE II. Comparison of InGaP and PPLN thin-film waveguides.

Platform	L (mm)	η_{SHG} (%/W/cm^2)	$\eta_{SHG}L^2$ (%/W)	χ (dB/$\sqrt{\text{mW}}$/cm)	χL (dB/$\sqrt{\text{mW}}$)
InGaP[33]	1.6	128 000	3 280	9.8	1.57
PPLN (uniform poling)[46]	4	2 600	416	1.4	0.56
PPLN (uniform poling)[47]	5	3 757	939	1.7	0.84
PPLN (adapted poling)[54]	21	2 150	9 500	1.3	2.67

TABLE III. Waveguide $\chi^{(2)}$ process. GVD: group velocity dispersion. $\alpha = \frac{1}{\pi}\sqrt{2\text{sinc}^{-1}\frac{1}{\sqrt{2}}}$. OPA: optical parametric amplification. PSA: phase-sensitive amplifier. PIA: phase-insensitive amplifier. $\epsilon = e^{-\gamma L}$: aggregated waveguide loss. The waveguide loss is only considered for the squeezed light.

$\chi^{(2)}$ process	Metric	Relation
SPDC	Pair generation efficiency	$\frac{\hbar\omega_p L^{3/2}}{12\sqrt{2\pi\left\|\text{GVD}\left(\frac{\omega_p}{2}\right)\right\|}}\chi^2$ (Ref. 55)
	Bandwidth	$\frac{\alpha}{\sqrt{\left\|\text{GVD}\left(\frac{\omega_p}{2}\right)\right\|L}}$ (Ref. 55)
OPA	Gain	$e^{\chi\sqrt{P_p}L}$ (maximum gain of PSA); $\frac{1}{4}e^{\chi\sqrt{P_p}L}$ (PIA)
	Bandwidth	$\frac{\alpha}{\sqrt{\left\|\text{GVD}\left(\frac{\omega_p}{2}\right)\right\|L}}$
Squeezed light	Squeeze ratio	$\epsilon\, e^{-\chi\sqrt{P_p}L} + 1 - \epsilon$ (Ref. 56)
Wavelength conversion	Conversion efficiency	$\sin^2\left(\chi\sqrt{P_p}L/\sqrt{2}\right)$

measuring the waveguide transmission. The normalized SHG efficiency of the phase-matched InGaP waveguide is measured to be 128 000%/W/cm^2,[33] which is consistent with the simulation value of 130 000%/W/cm^2. This is significantly higher than other demonstrations of InGaP $\chi^{(2)}$ nonlinear waveguides,[52,53] which are limited by considerable optical losses and imperfect phase matching. The normalized SHG efficiency of our InGaP nanophotonic waveguides is nearly two orders of magnitude higher than the thin-film periodically poled $LiNbO_3$ (PPLN) waveguides in the telecommunication band.[46,47,54] Such an enhancement in normalized nonlinear efficiency can be understood via a back-of-the-envelope calculation. The normalized SHG efficiency of the InGaP waveguide can be calculated using[33]

$$\eta_{SHG} \equiv \frac{P_{SHG}}{P_p^2 L^2} = \frac{\omega_a^2}{2n_a^2 n_b \epsilon_0 c^3}\left(\frac{\int d\mathbf{r}\chi^{(2)}_{xyz}\sum_{i\neq j\neq k}E^*_{bi}E_{aj}E_{ak}}{\int d\mathbf{r}|\mathbf{E}_a|^2\sqrt{\int d\mathbf{r}|\mathbf{E}_b|^2}}\right)^2, \quad (1)$$

where P_p is the pump power, L is the waveguide length, and the normalization integrals use electric field components perpendicular to the wavevector of the waveguide mode. Based on Eq. (1), the ratio between the normalized nonlinear efficiency of InGaP and PPLN waveguides is

estimated to be $(4 \times 2 \times \frac{\pi}{2})^2 \approx 160$, where $4\times$ is from $\chi^{(2)}_{xyz}$ of InGaP vs $\chi^{(2)}_{zzz}$ of $LiNbO_3$, $2\times$ is from the swap of indices x and y in $\chi^{(2)}_{xyz}$ for InGaP, and $1/\frac{2}{\pi}\times$ is due to the periodic poling of $LiNbO_3$. This estimation does not consider the difference in the mode overlap integral, which is generally an $O(1)$ factor. Table II summarizes the performance of InGaP and thin-film PPLN waveguides of recent demonstrations.[46,47,54] The SHG efficiency, $\eta_{\mathrm{SHG}}L^2$, of a 1–2 mm-long InGaP waveguide is higher than 4–5 mm-long PPLN waveguides with uniform poling[46,47] and is comparable to centimeter-long PPLN waveguides fabricated using the adapted poling technique.[54]

Using the normalized SHG efficiency, we can introduce a nonlinear gain defined as

$$\chi \equiv 2\sqrt{\eta_{\mathrm{SHG}}}. \tag{2}$$

The nonlinear gain is convenient to characterize second-order nonlinear optical processes in the waveguide, including optical parametric amplification and squeezed light generation. Table III summarizes the key metrics of several second-order nonlinear optical processes of the waveguide as functions of the nonlinear gain χ and waveguide loss. Figure 3(b) compares the nonlinear gain and waveguide loss of the InGaP platform with other $\chi^{(2)}$ nonlinear photonics platforms. In this plot, the numerical value of the nonlinear gain is calculated via $\chi\,[\mathrm{dB}/\sqrt{\mathrm{mW}}/\mathrm{cm}] = 10\log(e^{2\sqrt{\eta_{\mathrm{SHG}}}})$. The InGaP waveguide achieves $\chi = 9.8$ dB/$\sqrt{\mathrm{mW}}$/cm, which is significantly greater than other platforms. Comparison with the thin-film PPLN waveguides is provided in Table II.

IV. QUANTUM OPTICS: CAVITY

The nonlinearity-to-loss ratio of a few percent achieved in InGaP microring resonators enables quantum optical effects using passive bulk $\chi^{(2)}$ nonlinearity at the few- and single-photon levels. Creating quantum correlations between initially uncorrelated photons, such as photon antibunching and photon blockade, are fundamental quantum optical effects and useful quantum resources. This is usually achieved using quantum emitters[57] or quantum interference induced by ancillary pumps.[58] Recently, it was theoretically shown that photon antibunching and photon blockade can be achieved via passive bulk nonlinearities that are not necessarily in the strong coupling regime.[59] Consider two uncorrelated photons propagate through a waveguide-coupled $\chi^{(2)}$ nonlinear cavity. The wavefunction of the two photons after traversing the system consists of the nonlinear interaction-mediated amplitude T and the linear transmission amplitude t^2, where t is the single-photon transmission coefficient, leading to a normalized second-order correlation function,[59]

$$g^{(2)}(\tau) = \frac{|t_\omega^2 + T(\omega,\tau)|^2}{|t_\omega^2|^2}, \tag{3}$$

where ω denotes the frequency of the photons and $|T| \sim (g/\kappa)^2$. As a result, quantum correlations between photons, such as photon antibunching and photon blockade, can be achieved by controlling the single-photon transmission coefficient of the photonic circuit such that $t_\omega^2 + T(\omega,\tau) \approx 0$, even for $g/\kappa < 1$. Initial experimental demonstration of such an effect has been realized using a waveguide-coupled InGaP microring resonator,[60] where photon antibunching [i.e., $g^{(2)}(0) < g^{(2)}(\tau)$ for some τ] was observed. However, due to the free-standing InGaP device structure, thermal noises associated with the inherent mechanical vibrational modes of the device prevented the realization of photon blockade, i.e., $g^{(2)}(0) \approx 0$. We expect this issue to be solved by adopting the InGaP-on-insulator device structure, which is free of vibrational modes.

The highly nonlinear InGaP cavity also enables nonlinear-optical entangling operations that facilitate quantum communications and quantum networking. Existing quantum networking protocols, such as quantum teleportation and entanglement swapping, rely on linear-optical Bell state measurements to herald the distribution and transfer of quantum information. However, the linear-optical Bell state measurement necessitates identical photons, making them prone to errors from multiphoton emissions.[61,62] This dependency limits both the efficiency and fidelity of entanglement distribution. Additionally, any deviation in the input photons' identity can compromise the protocol's fidelity.[63,64] A solution to this issue is the nonlinear-optical Bell state measurement, which uses the sum-frequency generation (SFG) process to filter out multiphoton emissions. This approach also mitigates the need for quantum interference of identical photons; instead, the input photons only need to meet the phase-matching condition for sum-frequency generation. Deviations from this condition primarily impact efficiency rather than fidelity. Recently, as reported in Ref. 65, we demonstrated the nonlinear Bell state measurement by exploiting an InGaP nonlinear cavity with a single-photon SFG probability (4×10^{-5}) over three orders of magnitude beyond prior nonlinear waveguides.[66–69] Using the nanophotonic nonlinear Bell state analyzer, we achieved faithful quantum teleportation involving time-bin encoded, spectrally distinct photons with a fidelity $\geq 94\%$ down to the single-photon level and validated the robustness of this scheme against multiphoton emission. Beyond quantum teleportation, a nonlinear Bell state analyzer with even moderate SFG efficiency can facilitate faithful heralded entanglement swapping[70]—a crucial protocol for quantum repeaters—more efficiently than linear-optical protocols using ancillae.[71,72]

V. QUANTUM OPTICS: WAVEGUIDE

In this section, we analyze several nonlinear and quantum optical processes in waveguides and highlight the advantage of the InGaP

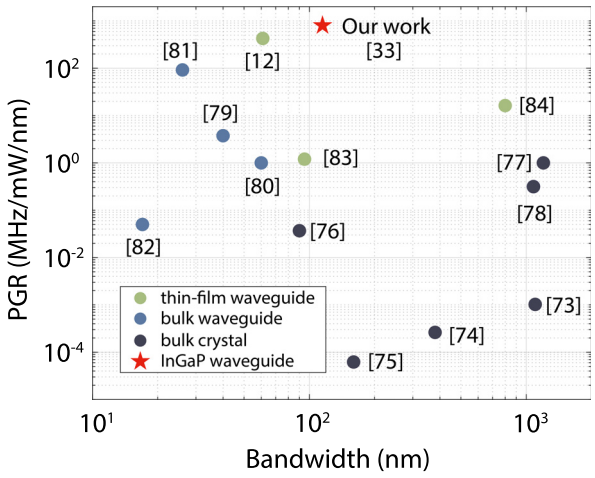

FIG. 4. Per-bandwidth pair generation rate (PGR) and bandwidth of recently demonstrated broadband SPDC sources. Bulk crystal,[73–78] bulk waveguide,[79–82] and thin-film waveguide.[12,33,83,84]

platform. One application of the $\chi^{(2)}$ nonlinear waveguide is for entangled photon pair generation via SPDC. The relations of the pair generation efficiency (P_{SPDC}/P_p) and the bandwidth of the SPDC photons of a phase-matched waveguide are given in Table III. Recently, we demonstrated an ultra-bright, broadband, time-energy entangled photon source utilizing the InGaP nanophotonic waveguide.[33] A 1.6 mm long InGaP waveguide achieves a pair generation rate of 97 GHz/mW and a bandwidth of 14.4 THz (115 nm) centered at the telecommunication C band. This corresponds to a per-bandwidth pair generation efficiency of 6.7 GHz/mW/THz (840 MHz/mW/nm). The ultrahigh rate efficiency of the InGaP nanophotonic waveguide can be understood from the fact that the pair generation efficiency is proportional to the SHG efficiency (Table III). In Fig. 4, we compare the InGaP nanophotonic waveguide SPDC source with other broadband SPDC sources, including bulk crystals and waveguides. The InGaP waveguide SPDC source exhibits a leading pair generation efficiency with a large bandwidth, underscoring its potential for quantum information applications.

Another application of $\chi^{(2)}$ nonlinear waveguides is for traveling-wave optical parametric amplifiers (OPAs). In this case, a pump light of frequency ω_p and a signal light of frequency ω_s, satisfying $\omega_p \approx 2\omega_s$, are injected into the $\chi^{(2)}$ nonlinear waveguide. When the waveguide satisfies the phase-matching condition, the three-wave mixing process transfers energy from the pump to amplify the signal. For a waveguide that is phase-matched for the degenerate three-wave mixing process, the bandwidth of the traveling-wave OPA is identical to that of the SPDC photons (Table III), determined by the waveguide length and the group velocity dispersion of the waveguide. When the frequencies of the pump and signal satisfy $\omega_p = 2\omega_s$, the OPA is phase-sensitive, i.e., the gain depends on the phase of the signal. In this case, the maximum gain is given by

$$G_{PSA} = e^{\chi\sqrt{P_p}L}, \tag{4}$$

where χ is the nonlinear gain introduced in Eq. (2), P_p is the pump power, and L is the length of the waveguide. When the frequencies of the pump and signal do not satisfy the double relationship and the signal lies in the phase-matching bandwidth, the OPA is phase-insensitive and the constant gain is given by

$$G_{PIA} = \cosh^2\left(\chi\sqrt{P_p}L/2\right) \approx \frac{1}{4}e^{\chi\sqrt{P_p}L}. \tag{5}$$

Essentially, the gain of a phase-insensitive OPA is 6 dB less than the maximum gain of a phase-sensitive OPA.[85] From the measured nonlinear gain $\chi = 9.8$ dB/$\sqrt{\text{mW}}$/cm of the InGaP waveguide, we expect a maximum gain of 30 dB can be achieved in a 1 cm long InGaP waveguide with only 10 mW on-chip pump power. The InGaP OPA empowered by its extreme $\chi^{(2)}$ nonlinearity is expected to transcend the state-of-the-art integrated traveling-wave OPAs based on Kerr nonlinearity,[86,87] in terms of pump efficiency, device size, and noise figure. To achieve this, phase mismatching due to film nonuniformity and power handling needs to be addressed (see Conclusion).

Related to the OPA, $\chi^{(2)}$ nonlinear waveguides can be used for generating squeezed light. When the waveguide is pumped at frequency ω_p, squeezed vacuum at the frequency of $\omega_p/2$ or two-mode squeezed light at frequencies $\omega_p/2 \pm \Delta$ can be generated. The quantum fluctuation of one quadrature of the squeezed vacuum (or the sum of one quadrature of the two-mode squeezed light) is deamplified, while that of the orthogonal quadrature (or the sum of the orthogonal quadrature) is amplified. Waveguide loss needs to be considered for the squeezed light since it corresponds to the vacuum noise. The squeeze ratio R, defined as the reduction of the quadrature noise power, of the squeezed vacuum and the two-mode squeezed light generated in a phase-matched $\chi^{(2)}$ nonlinear waveguide is given by[56]

$$R = \epsilon\, e^{-\chi\sqrt{P_p}L} + 1 - \epsilon, \tag{6}$$

where $\epsilon = e^{-\gamma L}$ is the aggregated waveguide loss. According to Eq. (6), for a given pump power, there exists an optimal waveguide length to achieve the maximum squeeze ratio, due to the trade-off between the parametric gain and waveguide loss. For example, using the measured nonlinear gain $\chi = 9.8$ dB/$\sqrt{\text{mW}}$/cm and waveguide loss of 0.8 dB/cm, for $P_p = 10(100)$ mW, an optimal squeezing of 9.5(13.5) dB can be achieved with a 5(2) mm long InGaP waveguide. This predicted squeezing level is significantly higher than current integrated squeezed light demonstrations using continuous-wave pumps, where the reported squeezing is around 2 dB (Refs. 56, 88–90) with one experiment reaching 6 dB,[91] and is comparable to the record of squeezing (15 dB) achieved using bulk nonlinear crystals.[92]

Finally, we consider quantum wavelength conversion using the InGaP nonlinear waveguide. To unify quantum platforms operating at different wavelengths and establish quantum networks utilizing optical fibers, quantum wavelength conversion of photons emitted by matter qubits to telecommunication C band photons is desirable. InGaP has a cutoff wavelength of 650 nm and low optical absorption below the bandgap, which makes it suitable for quantum wavelength conversion involving a variety of quantum emitters. We consider quantum wavelength conversion from quantum emitter wavelengths in the 670 – 1010 nm range to 1550 nm via different-frequency generation (DFG) with a pump wavelength longer than the emitter wavelength. We design InGaP-on-insulator (SiO_2) waveguides satisfying the

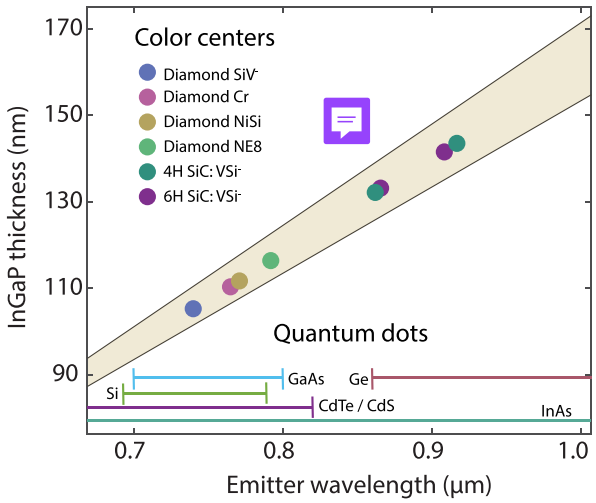

FIG. 5. Quantum wavelength conversion to 1550 nm through DFG for solid-state quantum emitters. Shaded area indicates the thickness of InGaP that realizes the phase-matching condition. The emission range of quantum dots is represented using line segments at the bottom. Defect color centers, diamond SiV,[93] diamond Cr,[93] diamond NiSi,[94,95] diamond NE8,[96] and V_{Si} in 4H SiC[97,98] and 6H SiC.[97] Quantum dots, InAs,[99] GaAs,[100,101] CdTe/CdS,[102] Si,[103] and Ge.[104]

phase-matching condition for such DFG processes. To this end, we limit the waveguide width to be in the range between 1 and 5 μm and identify the proper thickness of the InGaP such that the phase-matching condition can be realized for a given emitter wavelength. The shaded region in Fig. 5 shows the range of desired InGaP thickness depending on the emitter wavelength. Several solid-state defect centers and quantum dots emit in the wavelength range of 670–1010 nm considered here. For example, the SiV^- center in diamond has a zero phonon line (ZPL) at 740 nm (Ref. 105) and the two types of V_{Si}^- center in 4H-SiC have ZPL at 862 and 917 nm.[97,98] On the other hand, quantum dots can emit into a wide wavelength band depending on their composition and sizes, e.g., InAs (700–1200 nm),[99] GaAs (700–800 nm),[100,101] Si (693–789 nm),[103] CdTe/CdS (480–820 nm),[102] and Ge (860–1230 nm).[104] The quantum efficiency of wavelength conversion from the photon of wavelength λ_1 to the photon of target wavelength λ_2 is given by

$$F_{\lambda_2}(L)/F_{\lambda_1}(0) = \sin^2\left(\chi\sqrt{P_p}L/\sqrt{2}\right), \tag{7}$$

where $F_\lambda(x)$ is the photon number flux at position x and we have ignored waveguide loss. Thus, the waveguide length to achieve unit-efficiency conversion is

$$L_\pi = \pi/\left(\chi\sqrt{2P_p}\right). \tag{8}$$

Assuming the nonlinear gain of the waveguide for DFG is similar to that of the waveguide for SHG, we estimate $L_\pi = 3.1(9.8)$ mm for pump power $P_p = 10(1)$ mW. [illegible] pump powers for high-efficiency quantum wavelength conversion are significantly lower than the state of the art and will reduce parasitic noises that hamper quantum wavelength conversion.

VI. CONCLUSION

In this Perspective, we provided a brief review of the newly developed epitaxial InGaP integrated $\chi^{(2)}$ nonlinear photonics platform and discussed its applications in quantum and nonlinear optics. Leveraging its exceptional nonlinearity and low optical loss, the InGaP platform has achieved highly efficient $\chi^{(2)}$ nonlinear optical effects, surpassing the current state of the art, such as second-harmonic generation and entangled photon pair generation via SPDC. Additionally, the InGaP platform enables novel quantum optical effects at the few- and single-photon levels, which are crucial for quantum information processing and quantum networking. However, addressing certain challenges is necessary to fully realize the potential of the InGaP platform. The first challenge is to realize the InGaP-on-insulator platform, which will help mitigate parasitic noises for quantum optics and facilitate high optical powers for applications involving waveguide devices. Recently, the InGaP-on-insulator structure via low-temperature plasma-activated wafer bonding has been reported.[15] However, the reported optical loss is still worse than the suspended InGaP platform. Further optimization of the wafer bonding process to reduce optical losses is necessary. Another challenge is the thickness nonuniformity of the epitaxial InGaP thin film. The phase-matching condition for second-order nonlinear optical processes is highly sensitive to the InGaP thickness. This is in general not relevant for microcavities, as the thickness variation occurs at a much larger scale, but will impact waveguides with a considerable length, leading to reduced nonlinear efficiency. Growth condition optimization and the adapted waveguide approach[54] might be able to overcome this challenge. With these current obstacles addressed, the InGaP $\chi^{(2)}$ nonlinear photonics platform is expected to yield unparalleled performances for a broad range of classical and quantum applications, including optical parametric amplification, squeezed light generation, and quantum wavelength conversion, to name a few.

ACKNOWLEDGMENTS

This work was supported by the U.S. National Science Foundation (Grant No. ECCS-2223192), the NSF Quantum Leap Challenge Institute QLCI-HQAN (Grant No. 2016136), and the U. S. Department of Energy Office of Science National Quantum Information Science Research Centers.

AUTHOR DECLARATIONS

Conflict of Interest

The authors have no conflicts to disclose.

Author Contributions

Joshua Akin and Yunlei Zhao contributed equally to this work.

Joshua Akin: Writing – original draft (equal). **Yunlei Zhao:** Writing – original draft (equal). **A. K. M. Naziul Haque:** Writing – original draft (supporting). **Kejie Fang:** Project administration (equal).

DATA AVAILABILITY

All data used in this study are available from the corresponding authors upon reasonable request.

REFERENCES

[1] J. Anthony Giordmaine and R. C. Miller, "Tunable coherent parametric oscillation in $LiNbO_3$ at optical frequencies," Phys. Rev. Lett. **14**, 973 (1965).
[2] S. Ghimire, A. D. DiChiara, E. Sistrunk, P. Agostini, L. F. DiMauro, and D. A. Reis, "Observation of high-order harmonic generation in a bulk crystal," Nat. Phys. **7**, 138–141 (2011).
[3] Y. S. You, D. A. Reis, and S. Ghimire, "Anisotropic high-harmonic generation in bulk crystals," Nat. Phys. **13**, 345–349 (2017).
[4] P. G. Kwiat, K. Mattle, H. Weinfurter, A. Zeilinger, A. V. Sergienko, and Y. Shih, "New high-intensity source of polarization-entangled photon pairs," Phys. Rev. Lett. **75**, 4337 (1995).
[5] R. Schnabel, "Squeezed states of light and their applications in laser interferometers," Phys. Rep. **684**, 1–51 (2017).
[6] N. Gisin and R. Thew, "Quantum communication," Nat. Photonics **1**, 165–171 (2007).
[7] B. J. Lawrie, P. D. Lett, A. M. Marino, and R. C. Pooser, "Quantum sensing with squeezed light," ACS Photonics **6**, 1307–1318 (2019).
[8] J. L. O'brien, "Optical quantum computing," Science **318**, 1567–1570 (2007).
[9] A. Dutt, A. Mohanty, A. L. Gaeta, and M. Lipson, "Nonlinear and quantum photonics using integrated optical materials," Nat. Rev. Mater. **9**, 321–346 (2024).
[10] M. Ohashi, T. Kondo, R. Ito, S. Fukatsu, Y. Shiraki, K. Kumata, and S. S. Kano, "Determination of quadratic nonlinear optical coefficient of $Al_xGa_{1-x}As$ system by the method of reflected second harmonics," J. Appl. Phys. **74**, 596–601 (1993).
[11] C. P. Michael, K. Srinivasan, T. J. Johnson, O. Painter, K. H. Lee, K. Hennessy, H. Kim, and E. Hu, "Wavelength- and material-dependent absorption in GaAs and AlGaAs microcavities," Appl. Phys. Lett. **90**, 051108 (2007).

[12]M. Placke, J. Schlegel, F. Mann, P. D. Casa, A. Thies, M. Weyers, G. Tränkle, and S. Ramelow, "Telecom-band spontaneous parametric down-conversion in AlGaAs-on-insulator waveguides," Laser Photonics Rev. **18**, 2301293 (2024).
[13]L. Lin and J. Robertson, "Passivation of interfacial defects at III-V oxide interfaces," J. Vac. Sci. Technol. B **30**, 04E101 (2012).
[14]U. D. Dave, B. Kuyken, F. Leo, S.-P. Gorza, S. Combrie, A. De Rossi, F. Raineri, and G. Roelkens, "Nonlinear properties of dispersion engineered InGaP photonic wire waveguides in the telecommunication wavelength range," Opt. Express **23**, 4650–4657 (2015).
[15]L. Thiel, J. E. Castro, T. J. Steiner, C. L. Nguyen, A. Pechilis, L. Duan, N. Lewis, G. D. Cole, J. E. Bowers, and G. Moody, "Wafer-scale fabrication of ingap-on-insulator for nonlinear and quantum photonic applications," arXiv:2406.18788 (2024).
[16]T. Takamoto, M. Kaneiwa, M. Imaizumi, and M. Yamaguchi, "InGaP/GaAs-based multijunction solar cells," Prog. Photovoltaics. Res. Appl. **13**, 495–511 (2005).
[17]C. P. T. Svensson, T. Mårtensson, J. Trägårdh, C. Larsson, M. Rask, D. Hessman, L. Samuelson, and J. Ohlsson, "Monolithic GaAs/InGaP nanowire light emitting diodes on silicon," Nanotechnology **19**, 305201 (2008).
[18]J. Jiang, S. Tsao, T. O'sullivan, W. Zhang, H. Lim, T. Sills, K. Mi, M. Razeghi, G. J. Brown, and M. Z. Tidrow, "High detectivity InGaAs/InGaP quantum-dot infrared photodetectors grown by low pressure metalorganic chemical vapor deposition," Appl. Phys. Lett. **84**, 2166–2168 (2004).
[19]N. Pan, J. Elliott, M. Knowles, D. P. Vu, K. Kishimoto, J. K. Twynam, H. Sato, M. T. Fresina, and G. E. Stillman, "High reliability InGaP/GaAs HBT," IEEE Electron Device Lett. **19**, 115–117 (1998).
[20]H. Q. Zheng, S. F. Yoon, B. P. Gay, K. W. Mah, K. Radhakrishnan, and G. I. Ng, "Growth optimization of InGaP layers by solid source molecular beam epitaxy for the application of InGaP/$In_{0.2}Ga_{0.8}As$/GaAs high electron mobility transistor structures," J. Cryst. Growth **216**, 51–56 (2000).
[21]V. Eckhouse, I. Cestier, G. Eisenstein, S. Combrié, P. Colman, A. De Rossi, M. Santagiustina, C. G. Someda, and G. Vadalà, "Highly efficient four wave mixing in GaInP photonic crystal waveguides," Opt. Lett. **35**, 1440–1442 (2010).
[22]P. Colman, C. Husko, S. Combrié, I. Sagnes, C. W. Wong, and A. De Rossi, "Temporal solitons and pulse compression in photonic crystal waveguides," Nat. Photonics **4**, 862–868 (2010).
[23]U. D. Dave, C. Ciret, S.-P. Gorza, S. Combrie, A. De Rossi, F. Raineri, G. Roelkens, and B. Kuyken, "Dispersive-wave-based octave-spanning supercontinuum generation in InGaP membrane waveguides on a silicon substrate," Opt. Lett. **40**, 3584–3587 (2015).
[24]G. Marty, S. Combrié, F. Raineri, and A. De Rossi, "Photonic crystal optical parametric oscillator," Nat. Photonics **15**, 53–58 (2021).
[25]A. Chopin, A. Barone, I. Ghorbel, S. Combrié, D. Bajoni, F. Raineri, M. Galli, and A. De Rossi, "Ultra-efficient generation of time-energy entangled photon pairs in an InGaP photonic crystal cavity," Commun. Phys. **6**, 77 (2023).
[26]Y. Ueno, V. Ricci, and G. I. Stegeman, "Second-order susceptibility of $Ga_{0.5}In_{0.5}P$ crystals at 1.5 μm and their feasibility for waveguide quasi-phase matching," J. Opt. Soc. Am. B **14**, 1428–1436 (1997).
[27]D. J. Wilson, K. Schneider, S. Hönl, M. Anderson, Y. Baumgartner, L. Czornomaz, T. J. Kippenberg, and P. Seidler, "Integrated gallium phosphide nonlinear photonics," Nat. Photonics **14**, 57–62 (2020).
[28]A. Marandi, N. C. Leindecker, V. Pervak, R. L. Byer, and K. L. Vodopyanov, "Coherence properties of a broadband femtosecond mid-ir optical parametric oscillator operating at degeneracy," Opt. Express **20**, 7255–7262 (2012).
[29]M. Vainio and L. Halonen, "Mid-infrared optical parametric oscillators and frequency combs for molecular spectroscopy," Phys. Chem. Chem. Phys. **18**, 4266–4294 (2016).
[30]M. Razeghi and B.-M. Nguyen, "Advances in mid-infrared detection and imaging: A key issues review," Rep. Prog. Phys. **77**, 082401 (2014).
[31]Y. Yao, A. J. Hoffman, and C. F. Gmachl, "Mid-infrared quantum cascade lasers," Nat. Photonics **6**, 432–439 (2012).
[32]M. Zhao and K. Fang, "InGaP quantum nanophotonic integrated circuits with 1.5% nonlinearity-to-loss ratio," Optica **9**, 258–263 (2022).
[33]J. Akin, Y. Zhao, Y. Misra, A. N. Haque, and K. Fang, "InGaP $\chi^{(2)}$ integrated photonics platform for broadband, ultra-efficient nonlinear conversion and entangled photon generation," Light **13**, 290 (2024).
[34]B. Guha, F. Marsault, F. Cadiz, L. Morgenroth, V. Ulin, V. Berkovitz, A. Lemaître, C. Gomez, A. Amo, S. Combrié *et al.*, "Surface-enhanced gallium arsenide photonic resonator with quality factor of 6×10^6," Optica **4**, 218–221 (2017).
[35]J. Lu, M. Li, C.-L. Zou, A. Al Sayem, and H. X. Tang, "Toward 1% single-photon anharmonicity with periodically poled lithium niobate microring resonators," Optica **7**, 1654–1659 (2020).
[36]J.-Y. Chen, Z.-H. Ma, Y. M. Sua, Z. Li, C. Tang, and Y.-P. Huang, "Ultra-efficient frequency conversion in quasi-phase-matched lithium niobate microrings," Optica **6**, 1244–1245 (2019).
[37]X. Guo, C.-L. Zou, and H. X. Tang, "Second-harmonic generation in aluminum nitride microrings with 2500%/w conversion efficiency," Optica **3**, 1126–1131 (2016).
[38]X. Guo, C-l Zou, C. Schuck, H. Jung, R. Cheng, and H. X. Tang, "Parametric down-conversion photon-pair source on a nanophotonic chip," Light **6**, e16249–e16249 (2016).
[39]D. F. Walls and G. J. Milburn, *Quantum Optics* (Springer Science & Business Media, 2007).
[40]Z. Ma, J.-Y. Chen, Z. Li, C. Tang, Y. M. Sua, H. Fan, and Y.-P. Huang, "Ultrabright quantum photon sources on chip," Phys. Rev. Lett. **125**, 263602 (2020).
[41]P. S. Kuo, J. Bravo-Abad, and G. S. Solomon, "Second-harmonic generation using-quasi-phasematching in a GaAs whispering-gallery-mode microcavity," Nat. Commun. **5**, 3109 (2014).
[42]L. Chang, A. Boes, P. Pintus, J. D. Peters, M. J. Kennedy, X.-W. Guo, N. Volet, S.-P. Yu, S. B. Papp, and J. E. Bowers, "Strong frequency conversion in heterogeneously integrated GaAs resonators," APL Photonics **4**, 036103 (2019).
[43]A. W. Bruch, X. Liu, X. Guo, J. B. Surya, Z. Gong, L. Zhang, J. Wang, J. Yan, and H. X. Tang, "17 000%/W second-harmonic conversion efficiency in single-crystalline aluminum nitride microresonators," Appl. Phys. Lett. **113**, 131102 (2018).
[44]S. Mariani, A. Andronico, A. Lemaître, I. Favero, S. Ducci, and G. Leo, "Second-harmonic generation in AlGaAs microdisks in the telecom range," Opt. Lett. **39**, 3062–3065 (2014).
[45]A. D. Logan, M. Gould, E. R. Schmidgall, K. Hestroffer, Z. Lin, W. Jin, A. Majumdar, F. Hatami, A. W. Rodriguez, and K.-M. C. Fu, "400%/W second harmonic conversion efficiency in 14 μm-diameter gallium phosphide-on-oxide resonators," Opt. Express **26**, 33687–33699 (2018).
[46]C. Wang, C. Langrock, A. Marandi, M. Jankowski, M. Zhang, B. Desiatov, M. M. Fejer, and M. Lončar, "Ultrahigh-efficiency wavelength conversion in nanophotonic periodically poled lithium niobate waveguides," Optica **5**, 1438–1441 (2018).
[47]J. Zhao, M. Rüsing, U. A. Javid, J. Ling, M. Li, Q. Lin, and S. Mookherjea, "Shallow-etched thin-film lithium niobate waveguides for highly-efficient second-harmonic generation," Opt. Express **28**, 19669–19682 (2020).
[48]S. May, M. Kues, M. Clerici, and M. Sorel, "Second-harmonic generation in AlGaAs-on-insulator waveguides," Opt. Lett. **44**, 1339–1342 (2019).
[49]K. Pantzas, S. Combrié, M. Bailly, R. Mandouze, F. R. Talenti, A. Harouri, B. Gérard, G. Beaudoin, L. Le Gratiet, G. Patriarche *et al.*, "Continuous-wave second-harmonic generation in orientation-patterned gallium phosphide waveguides at telecom wavelengths," ACS Photonics **9**, 2032–2039 (2022).
[50]Y. Zheng, A. Yi, C. Ye, K. Yvind, H. Zhang, X. Ou, and M. Pu, "Efficient second-harmonic generation in silicon carbide nanowaveguides," in *Conference on Lasers and Electro-Optics (CLEO)* (IEEE, 2022), pp. 1–2.
[51]A. Yi, C. Wang, L. Zhou, Y. Zhu, S. Zhang, T. You, J. Zhang, and X. Ou, "Silicon carbide for integrated photonics," Appl. Phys. Rev. **9**, 031302 (2022).
[52]N. Poulvellarie, C. Mas Arabi, C. Ciret, S. Combrié, A. De Rossi, M. Haelterman, F. Raineri, B. Kuyken, S.-P. Gorza, and F. Leo, "Efficient type II second harmonic generation in an indium gallium phosphide on insulator wire waveguide aligned with a crystallographic axis," Opt. Lett. **46**, 1490–1493 (2021).
[53]A. Peralta Amores and M. Swillo, "Low temperature bonding of nanolayered InGaP/SiO_2 waveguides for spontaneous-parametric down conversion," ACS Appl. Nano Mater. **5**, 2550–2557 (2022).
[54]P.-K. Chen, I. Briggs, C. Cui, L. Zhang, M. Shah, and L. Fan, "Adapted poling to break the nonlinear efficiency limit in nanophotonic lithium niobate waveguides," Nat. Nanotechnol. **19**, 44–50 (2024).

[55]R. Kumar and J. Ghosh, "Parametric down-conversion in ppLN ridge waveguide: A quantum analysis for efficient twin photons generation at 1550 nm," J. Opt. **20**, 075202 (2018).
[56]H. S. Stokowski, T. P. McKenna, T. Park, A. Y. Hwang, D. J. Dean, O. T. Celik, V. Ansari, M. M. Fejer, and A. H. Safavi-Naeini, "Integrated quantum optical phase sensor in thin film lithium niobate," Nat. Commun. **14**, 3355 (2023).
[57]K. M. Birnbaum, A. Boca, R. Miller, A. D. Boozer, T. E. Northup, and H. Jeff Kimble, "Photon blockade in an optical cavity with one trapped atom," Nature **436**, 87–90 (2005).
[58]H. Flayac and V. Savona, "Unconventional photon blockade," Phys. Rev. A **96**, 053810 (2017).
[59]Y. Wang and K. Fang, "Few-photon transport via a multimode nonlinear cavity: Theory and applications," Phys. Rev. A **105**, 023713 (2022).
[60]M. Zhao, Y. Wang, S. Fan, and K. Fang, "Quantum correlated photons via a passive nonlinear microcavity," arXiv:2304.11676 (2023).
[61]P. Kok and S. L. Braunstein, "Postselected versus nonpostselected quantum teleportation using parametric down-conversion," Phys. Rev. A **61**, 042304 (2000).
[62]J.-W. Pan, S. Gasparoni, M. Aspelmeyer, T. Jennewein, and A. Zeilinger, "Experimental realization of freely propagating teleported qubits," Nature **421**, 721–725 (2003).
[63]N. Sangouard, C. Simon, H. De Riedmatten, and N. Gisin, "Quantum repeaters based on atomic ensembles and linear optics," Rev. Mod. Phys. **83**, 33–80 (2011).
[64]K. Azuma, S. E. Economou, D. Elkouss, P. Hilaire, L. Jiang, H.-K. Lo, and I. Tzitrin, "Quantum repeaters: From quantum networks to the quantum internet," Rev. Mod. Phys. **95**, 045006 (2023).
[65]J. Akin, Y. Zhao, P. G. Kwiat, E. A. Goldschmidt, and K. Fang, "Faithful quantum teleportation via a nanophotonic nonlinear bell state analyzer," arXiv:2411.15437 (2024).
[66]S. Tanzilli, W. Tittel, M. Halder, O. Alibart, P. Baldi, N. Gisin, and H. Zbinden, "A photonic quantum information interface," Nature **437**, 116–120 (2005).
[67]T. Guerreiro, E. Pomarico, B. Sanguinetti, N. Sangouard, J. S. Pelc, C. Langrock, M. M. Fejer, H. Zbinden, R. T. Thew, and N. Gisin, "Interaction of independent single photons based on integrated nonlinear optics," Nat. Commun. **4**, 2324 (2013).
[68]T. Guerreiro, A. Martin, B. Sanguinetti, J. S. Pelc, C. Langrock, M. M. Fejer, N. Gisin, H. Zbinden, N. Sangouard, and R. T. Thew, "Nonlinear interaction between single photons," Phys. Rev. Lett. **113**, 173601 (2014).
[69]P. Fisher, R. Cernansky, B. Haylock, and M. Lobino, "Single photon frequency conversion for frequency multiplexed quantum networks in the telecom band," Phys. Rev. Lett. **127**, 023602 (2021).
[70]N. Sangouard, B. Sanguinetti, N. Curtz, N. Gisin, R. Thew, and H. Zbinden, "Faithful entanglement swapping based on sum-frequency generation," Phys. Rev. Lett. **106**, 120403 (2011).
[71]C. Wagenknecht, C.-M. Li, A. Reingruber, X.-H. Bao, A. Goebel, Y.-A. Chen, Q. Zhang, K. Chen, and J.-W. Pan, "Experimental demonstration of a heralded entanglement source," Nat. Photonics **4**, 549–552 (2010).
[72]S. Barz, G. Cronenberg, A. Zeilinger, and P. Walther, "Heralded generation of entangled photon pairs," Nat. Photonics **4**, 553–556 (2010).
[73]A. Tanaka, R. Okamoto, H. H. Lim, S. Subashchandran, M. Okano, L. Zhang, L. Kang, J. Chen, P. Wu, T. Hirohata *et al.*, "Noncollinear parametric fluorescence by chirped quasi-phase matching for monocycle temporal entanglement," Opt. Express **20**, 25228–25238 (2012).
[74]M. Okano, H. H. Lim, R. Okamoto, N. Nishizawa, S. Kurimura, and S. Takeuchi, "0.54 μm resolution two-photon interference with dispersion cancellation for quantum optical coherence tomography," Sci. Rep. **5**, 18042 (2015).
[75]M. Okano, R. Okamoto, A. Tanaka, S. Subashchandran, and S. Takeuchi, "Generation of broadband spontaneous parametric fluorescence using multiple bulk nonlinear crystals," Opt. Express **20**, 13977–13987 (2012).
[76]M. V. Chekhova, S. Germanskiy, D. B. Horoshko, G. K. Kitaeva, M. I. Kolobov, G. Leuchs, C. R. Phillips, and P. A. Prudkovskii, "Broadband bright twin beams and their upconversion," Opt. Lett. **43**, 375–378 (2018).
[77]Y. Shaked, R. Pomerantz, R. Z. Vered, and A. Peer, "Observing the nonclassical nature of ultra-broadband bi-photons at ultrafast speed," New J. Phys. **16**, 053012 (2014).
[78]K. A. O'Donnell and A. B. U'Ren, "Observation of ultrabroadband, beamlike parametric downconversion," Opt. Lett. **32**, 817–819 (2007).
[79]S. Tanzilli, W. Tittel, H. De Riedmatten, H. Zbinden, P. Baldi, M. DeMicheli, D. B. Ostrowsky, and N. Gisin, "PPLN waveguide for quantum communication," Eur. Phys. J. D **18**, 155–160 (2002).
[80]Y. Huang, J. Feng, Y. Li, Z. Qi, C. Lu, Y. Zheng, and X. Chen, "High-performance hyperentanglement generation and manipulation based on lithium niobate waveguides," Phys. Rev. Appl. **17**, 054002 (2022).
[81]B. Cao, K. Hayama, S. Suezawa, M. Hisamitsu, K. Tokuda, S. Kurimura, R. Okamoto, and S. Takeuchi, "Non-collinear generation of ultra-broadband parametric fluorescence photon pairs using chirped quasi-phase matching slab waveguides," Opt. Express **31**, 23551–23562 (2023).
[82]A. B. U'Ren, C. Silberhorn, K. Banaszek, and I. A. Walmsley, "Efficient conditional preparation of high-fidelity single photon states for fiber-optic quantum networks," Phys. Rev. Lett. **93**, 093601 (2004).
[83]D. Kang, A. Anirban, and A. S. Helmy, "Monolithic semiconductor chips as a source for broadband wavelength-multiplexed polarization entangled photons," Opt. Express **24**, 15160–15170 (2016).
[84]U. A. Javid, J. Ling, J. Staffa, M. Li, Y. He, and Q. Lin, "Ultrabroadband entangled photons on a nanophotonic chip," Phys. Rev. Lett. **127**, 183601 (2021).
[85]P. A. Andrekson and M. Karlsson, "Fiber-based phase-sensitive optical amplifiers and their applications," Adv. Opt. Photonics **12**, 367–428 (2020).
[86]J. Riemensberger, N. Kuznetsov, J. Liu, J. He, R. N. Wang, and T. J. Kippenberg, "A photonic integrated continuous-travelling-wave parametric amplifier," Nature **612**, 56–61 (2022).
[87]N. Kuznetsov, A. Nardi, A. Davydova, M. Churaev, J. Riemensberger, P. Seidler, and T. J. Kippenberg, "An ultra-broadband photonic-chip-based traveling-wave parametric amplifier," arXiv:2404.08609 (2024).
[88]F. Mondain, T. Lunghi, A. Zavatta, E. Gouzien, F. Doutre, M. De Micheli, S. Tanzilli, and V. D'Auria, "Chip-based squeezing at a telecom wavelength," Photonics Res. **7**, A36–A39 (2019).
[89]A. Dutt, K. Luke, S. Manipatruni, A. L. Gaeta, P. Nussenzveig, and M. Lipson, "On-chip optical squeezing," Phys. Rev. Appl. **3**, 044005 (2015).
[90]Y. Zhao, Y. Okawachi, J. K. Jang, X. Ji, M. Lipson, and A. L. Gaeta, "Near-degenerate quadrature-squeezed vacuum generation on a silicon-nitride chip," Phys. Rev. Lett. **124**, 193601 (2020).
[91]T. Kashiwazaki, N. Takanashi, T. Yamashima, T. Kazama, K. Enbutsu, R. Kasahara, T. Umeki, and A. Furusawa, "Continuous-wave 6-dB-squeezed light with 2.5-THz-bandwidth from single-mode PPLN waveguide," APL Photonics **5**, 036104 (2020).
[92]H. Vahlbruch, M. Mehmet, K. Danzmann, and R. Schnabel, "Detection of 15 dB squeezed states of light and their application for the absolute calibration of photoelectric quantum efficiency," Phys. Rev. Lett. **117**, 110801 (2016).
[93]I. Aharonovich and E. Neu, "Diamond nanophotonics," Adv. Opt. Mater. **2**, 911–928 (2014).
[94]D. Steinmetz, E. Neu, J. Meijer, W. Bolse, and C. Becher, "Single photon emitters based on Ni/Si related defects in single crystalline diamond," Appl. Phys. B **102**, 451–458 (2011).
[95]J. R. Rabeau, Y. L. Chin, S. Prawer, F. Jelezko, T. Gaebel, and J. Wrachtrup, "Fabrication of single nickel-nitrogen defects in diamond by chemical vapor deposition," Appl. Phys. Lett. **86**, 131926 (2005).
[96]T. Gaebel, I. Popa, A. Gruber, M. Domhan, F. Jelezko, and J. Wrachtrup, "Stable single-photon source in the near infrared," New J. Phys. **6**, 98 (2004).
[97]E. Sörman, N. T. Son, W. M. Chen, O. Kordina, C. Hallin, and E. Janzén, "Silicon vacancy related defect in 4H and 6H SiC," Phys. Rev. B **61**, 2613–2620 (2000).
[98]N. T. Son, C. P. Anderson, A. Bourassa, K. C. Miao, C. Babin, M. Widmann, M. Niethammer, J. Ul Hassan, N. Morioka, I. G. Ivanov, F. Kaiser, J. Wrachtrup, and D. D. Awschalom, "Developing silicon carbide for quantum spintronics," Appl. Phys. Lett. **116**, 190501 (2020).
[99]D. Franke, D. K. Harris, O. Chen, O. T. Bruns, J. A. Carr, M. W. B. Wilson, and M. G. Bawendi, "Continuous injection synthesis of indium arsenide

quantum dots emissive in the short-wavelength infrared," Nat. Commun. **7**, 12749 (2016).
[100]C. Heyn, A. Stemmann, T. Köppen, C. Strelow, T. Kipp, M. Grave, S. Mendach, and W. Hansen, "Highly uniform and strain-free GaAs quantum dots fabricated by filling of self-assembled nanoholes," Appl. Phys. Lett. **94**, 183113 (2009).
[101]L. Zhai, M. C. Löbl, G. N. Nguyen, J. Ritzmann, A. Javadi, C. Spinnler, A. D. Wieck, A. Ludwig, and R. J. Warburton, "Low-noise GaAs quantum dots for quantum photonics," Nat. Commun. **11**, 4745 (2020).
[102]Z. Deng, O. Schulz, S. Lin, B. Ding, X. Liu, X. Wei, R. Ros, H. Yan, and Y. Liu, "Aqueous synthesis of zinc blende CdTe/CdS magic-core/thick-shell tetrahedral-shaped nanocrystals with emission tunable to near-infrared," J. Am. Chem. Soc. **132**, 5592–5593 (2010).
[103]D. Jurbergs, E. Rogojina, L. Mangolini, and U. Kortshagen, "Silicon nanocrystals with ensemble quantum yields exceeding 60%," Appl. Phys. Lett. **88**, 233116 (2006).
[104]D. A. Ruddy, J. C. Johnson, E. R. Smith, and N. R. Neale, "Size and bandgap control in the solution-phase synthesis of near-infrared-emitting germanium nanocrystals," ACS Nano **4**, 7459–7466 (2010).
[105]T. Feng and B. D. Schwartz, "Characteristics and origin of the 1.681 eV luminescence center in chemical–vapor–deposited diamond films," J. Appl. Phys. **73**, 1415–1425 (1993).